Publishing House
AKAPIT

COMPUTER METHODS IN MATERIALS SCIENCE

Informatyka w Technologii Materiałów

Vol. 13, 2013, No. 1

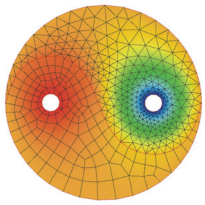

SIMULATION OF THE TEMPERATURE FIELD AND THE MICROSTRUCTURE EVOLUTION DURING MULTI-PASS WELDING OF L485MB PIPELINE STEEL

FELIX KOCH[1], MARCO ENDERLEIN[1], MACIEJ PIETRZYK[2]

[1] Technische Universität Bergakademie Freiberg, Institute of Mechanics and Fluid Dynamics
Lampadiusstraße 4, 09599 Freiberg, Germany
[2] AGH University of Science and Technology, Al. Mickiewicza 30, 30-059 Kraków, Poland
**Corresponding author: Felix.Koch@imfd.tu-freiberg.de*

Abstract

Against the background of safety assessment of welded joints in piping constructions, the welding process is simulated numerically in the present work. The paper focuses on manual multi-pass edge fillet welds at high-pressure pipelines made of steel L485MB (X70). The simulation is based on the finite element method and allows for the prediction of temperature fields and microstructure evolution during welding and cooling. To describe the heat input during welding the double-ellipsoidal Goldak heat source is implemented into the commercial software ABAQUS. To account for different bead shapes the Goldak heat source is modified by projecting it onto the bead shape of each welding pass. The microstructure evolution is analyzed by a phase transformation model based on the calculated transient temperature fields. The ferritic, pearlitic and bainitic transformations are simulated by the Avrami equation. Effects of reheating during multi-pass welding are taken into account. In order to validate the simulation extensive welding experiments are carried out. The experimental observations are presented and compared to the numerical results by means of macrosections and thermocouple measurements.

Key words: multi-pass welding, temperature field, microstructure, pipeline, L485MB, X70

1. INTRODUCTION

If gas pipelines should be repaired or extended the gas flow cannot be stopped in most cases to ensure service without interruption. For safety reasons the necessary welding work require a very sensitive and adapted heat management, to prevent burn through and accelerated cooling of the welds. Preheating is used to compensate the heat loss through the pipe wall due to the gas flow. Cooling of the welds is therefore slowed down and martensite formation as well as cold cracking within the heat affected zone (HAZ) can be avoided. In the present work the steel L485MB is considered, which is commonly used for large-diameter pipes carrying gas or liquids under high pressure. Experimental observations of Li et al. (2011) and Lan et al. (2011) show, that the mechanical properties of L485MB in the heat affected zone are mainly influenced by the cooling time after welding. Especially hardness increase is found with decreasing cooling time. To improve safety and quality of such welds, the temperature field and the evolution of microstructure during welding of L485MB are simulated in the present work using the finite element method and a phase transformation model based on Donnay et al. (1996). The modelling and simulation procedure to compute the temperature field during welding is based on the work of Koch and Enderlein (2012).

ISSN 1641-8581

The calculated transient temperature field is used as an input for the phase transformation model, which is capable to predict the susceptibility of martensite formation in the HAZ.

2. MODELLING ABSTRACTIONS

2.1. Temperature field computation

The thermal cycle during welding is simulated using the finite element method (FEM). That means, the field equation of transient heat conduction is solved numerically:

$$\frac{\partial T}{\partial t} = \frac{\lambda}{c\rho}\left(\frac{\partial^2 T}{\partial x^2} + \frac{\partial^2 T}{\partial y^2} + \frac{\partial^2 T}{\partial z^2}\right) + \frac{1}{c\rho} q^{vol} \qquad (1)$$

where: T – temperature, t – time, x, y, z – coordinates fixed in space, λ – thermal conductivity, c – specific heat capacity, ρ – density (λ, c, ρ are temperature dependent).

The heat input during welding is modelled with the Goldak heat source q^{vol} (Goldak & Akhlaghi, 2005). It is a power density distribution depending on the heat input by the welding arc and the coordinates x', y', z' moving together with the heat source (figure 1). To consider the bead appearance of each welding pass the Goldak heat source is projected onto the bead shape as described by Koch and Enderlein (2012). Equation (1) is solved within a limited body. The corresponding thermal initial - boundary value problem is illustrated in figure 1.

The initial temperature T_0 is prescribed for the whole calculation domain. The heat transfer via convection $\bar{q}^{con.}$ and radiation $\bar{q}^{rad.}$ is considered at the boundary S (figure 1):

$$\begin{aligned} \bar{q}^{con.} &= \alpha\left(T_S - T_{amb.}\right) \\ \bar{q}^{rad.} &= \varepsilon\sigma_B\left(T_S^4 - T_{amb.}^4\right) \end{aligned} \qquad (2)$$

where: α – heat transfer coefficient, T_S – surface temperature, $T_{amb.}$ – ambient temperature, ε – emissivity, σ_B – Boltzmann constant.

The air gap between the parts to be joined is accounted for with the conductive and radiative heat exchange between the gap surfaces SA and SB. The corresponding fluxes $\bar{q}^{con.\,gap}$ and $\bar{q}^{rad.\,gap}$ are defined according to Baehr and Stephan (2011) and Nishida et al. (1986):

$$\begin{aligned} \bar{q}^{con.\,gap} &= \frac{\lambda}{d}\left(T_{gap\,SA} - T_{gap\,SB}\right) \\ \bar{q}^{rad.\,gap} &= \frac{\sigma_B}{1/\varepsilon_{gap\,SA} + 1/\varepsilon_{gap\,SB} - 1}\left(T_{gap\,SA}^4 - T_{gap\,SB}^4\right) \end{aligned} \qquad (3)$$

where: λ – conductivity of air (temperature dependent), d – gap width, $T_{gap\,SA/B}$ – temperature of the gap surface, $\varepsilon_{gap\,SA/B}$ - emissivity of the gap surface.

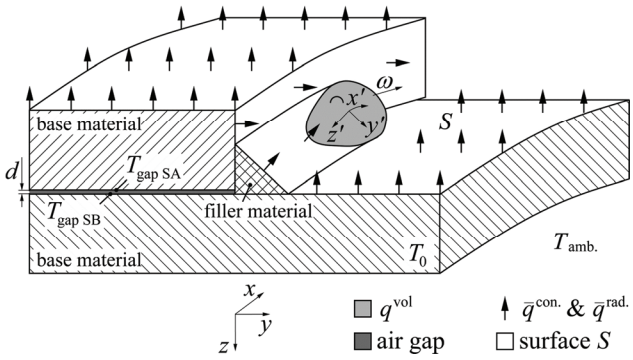

Fig. 1. *Thermal initial – boundary value problem for the single-pass edge fillet weld.*

2.2. Prediction of the microstructure evolution

The phase transformation model for the investigated steel was determined and reduced using sensitivity analysis (Szeliga, 2012). Inverse analysis for dilatometric tests was applied to identify coefficients in the model. The chemical composition of the steel is given in table 1.

Table 1. *Chemical composition of the investigated bainitic steel L485MB, wt%*

C	Si	Mn	P	S	Cr	B	Ti	Ni	Al	Cu
0.115	0.485	1.6	0.02	0.0175	0.1	0.003	0.11	0.16	0.034	0.16

The model proposed by Donnay et al. (1996) is based on the Avrami (1939) equation:

$$X = 1 - \exp(-kt^n) \qquad (4)$$

where: X – transformed volume fraction, k, n – coefficients.

Theoretical considerations show that, according to the type of transformation (nucleation and growth, site saturation) a constant value of n in equation (4) can be used. On contrary, value of the coefficient k must vary with temperature in a way linked to the form of a transformation-time-temperature (TTT) diagram. A modified Gaussian function proposed by Donnay et al. (1996) is used for the ferritic transformation in the present work:

$$k = k_{\max} \exp\left[-\left(\frac{T - T_{nose}}{a_8} \right)^{a_7} \right] \quad (5)$$

In equation (5) T_{nose} is the temperature of the maximum at the Gauss function and k_{max} is the maximum value of this function. Investigation has shown that the following equations describe well k for pearlitic and bainitic transformations:

$$k = \frac{a_{14}}{D_\gamma^{a_{16}}} \exp\left(a_{13} - a_{12} T \right) \text{ (pearlitic)} \quad (6)$$

$$k = a_{23} \left(a_{22} - a_{21} T \right) \text{ (bainitic)} \quad (7)$$

Incubation times for all transformations were widely investigated and are calculated as:

$$\tau_P = \frac{a_9}{\left(\mathrm{Ae}_1 - T \right)^{a_{11}}} \exp\left(\frac{a_{10}}{R\hat{T}} \right) \text{ (pearlitic)} \quad (8)$$

$$\tau_b = \frac{a_{17}}{\left(T_b - T \right)^{a_{19}}} \exp\left(\frac{a_{18}}{R\hat{T}} \right) \text{ (bainitic)} \quad (9)$$

where: D_γ – austenite grain size, T – temperature in °C, $\hat{T}$ – temperature in K, R – gas constant.

Start temperatures for the bainitic (T_b) and martensitic (T_m) transformations are functions of steel composition (table 1):

$$T_b[^\circ\mathrm{C}] = a_{20} - 425[\mathrm{C}] - 42.5[\mathrm{Mn}] - 31.5[\mathrm{Ni}] \quad (10)$$

$$T_m[^\circ\mathrm{C}] = a_{26} - a_{27} C_\gamma \quad (11)$$

where: C_γ - average carbon concentration in the austenite.

Modelling of phase transformations in the heating part of the thermal cycle during welding process is presented eg. by Zhang et al. (2005). In the present work the model based on the Avrami equation (4) is used. Incubation time is calculated using the following equation:

$$\tau_h = \frac{a_1}{\left(T - A_{e1} \right)^{a_3}} \exp\left(\frac{a_2}{R\hat{T}} \right) \quad (12)$$

Scheil (1935) additivity rule is used to account for the temperature changes during both incubation time and progress of the transformation. When the incubation time is finished, kinetics of the transformation into austenite is calculated using equation (4). Coefficient k in this equation is introduced as a following function of temperature.

$$k = k_{PBM} a_{28} \exp\left(\frac{-a_{29}}{R\hat{T}} \right) \quad (13)$$

A_{e3} and A_{e1} are equilibrium temperatures determined using ThermoCalc software. This model for heating contains 6 coefficients, a_1, a_2 and a_3 in equation (12) describing incubation time and a_{28} and a_{29} in equation (13) describing kinetics of transformation. Coefficient k_{PBM} in equation (13) accounts for the influence of the pearlite, bainite and martensite on the kinetics of transformation. This coefficient is equal 1 during ferrite to austenite transformation.

Coefficients in the whole phase transformation model were determined using inverse analysis of dilatometric tests, see Pietrzyk and Kuziak (2012) for description of the algorithm. Values of the coefficients are given in Pietrzyk et al. (2010).

3. EXPERIMENTAL APPROACH

The three pass edge fillet weld is carried out connecting two curved plates (L485MB) by manual metal arc welding (MMAW). The specimen is a 20° section (arc length of 190 mm) of the pipeline and the T-fitting. It is taken from a pipe with nominal diameter of 1100 mm. The experimental set-up is illustrated in figure 2. The pipeline plate is located in a suspension which is connected to the ground terminal of the welding machine. The T-fitting plate is fixed onto the pipeline plate by tack welds. Natural convection can be assumed all around the specimen, due to the design of the suspension.

The specimen is preheated to 50°C before welding. Rutile basic coated electrodes are used with a core wire diameter of 3.2 mm (EN499 E38 2 RB 1 2). The slag resulting from the electrode burn-off is removed from each layer after welding. Temperature time curves are recorded at the measurement loops one to eight by thermowires (NiCr-Ni). The thermowires are spotwelded to the specimen surface. The welding process parameters (I_{rms}, U_{rms}, t^{weld}) are measured online by the process sensor HKS P1000 (table 2). A macrosection is prepared at position r_2 = 60 mm in order to obtain the bead shape, the fusion line and the HAZ.

Table 2. *Welding parameters for the three pass edge fillet weld*

layer	I_{rms} [A]	U_{rms} [V]	P [W]	t^{weld} [s]	s [mm]	v [mm/s]	E [Ws/mm]	t^C [s]
1	144.4	23.0	3321.2	47.3	190	3.91	849.4	129.7
2	144.7	23.3	3371.5	34.4	175	5.39	625.5	87.6
3	144.7	23.7	3429.4	26.0	110	4.38	790.2	1400.0
s – weld length, $E = U_{rms} \cdot I_{rms}/v$ (energy per unit length), t^C – cooling time.								

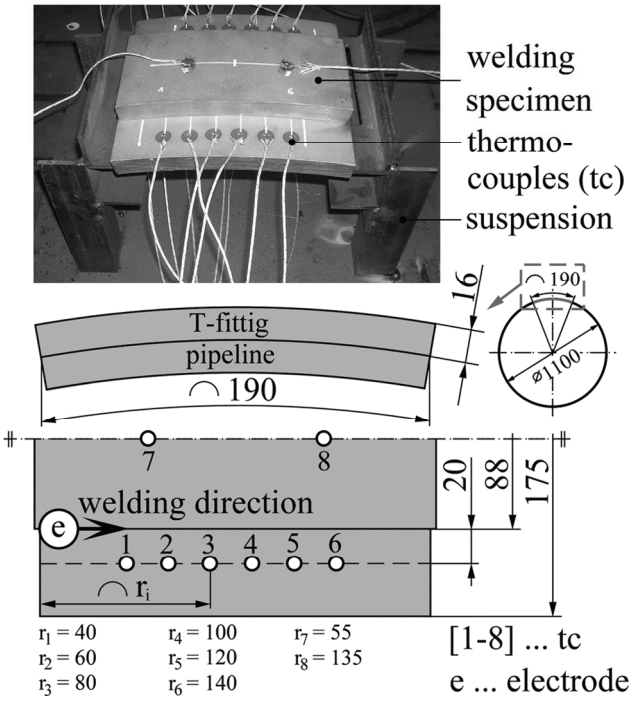

Fig. 2. *Experimental set-up for the edge fillet weld (all dimensions in mm).*

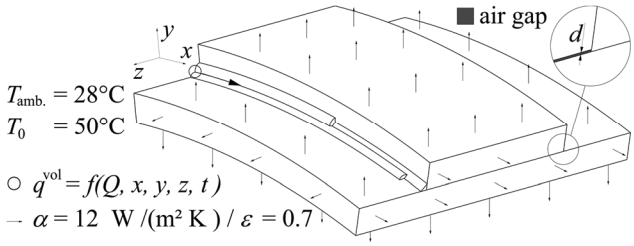

Fig. 3. *ABAQUS FE-model for the three pass edge fillet weld with boundary conditions.*

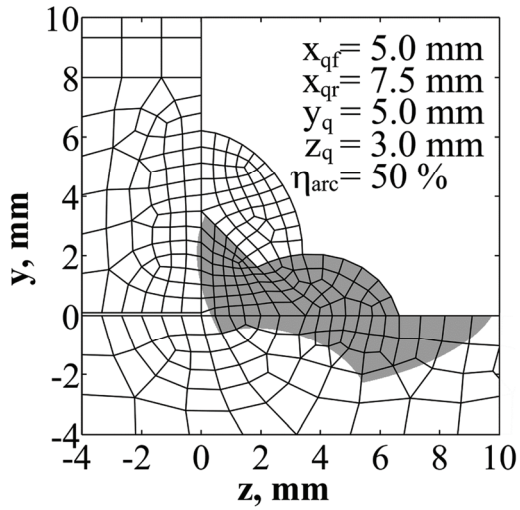

(a) Mesh and heat source domain (gray)

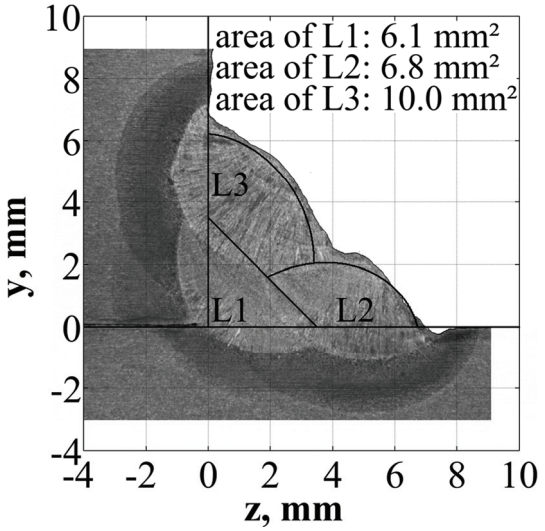

(b) Macrosection

Fig. 4. *Modelling of the bead shape (L1 = first layer, L2 = second layer, L3 = third layer).*

4. FE-MODEL

The thermal field during welding and cooling of the specimen is computed using the finite element (FE) software ABAQUS. An overview of the applied FE-model as well as the boundary conditions is given in figure 3. The FE-model includes the plates to be connected and the three welding layers. The air gap between the plates is taken into consideration with an average gap width d = 0.1 mm. The initial temperature T_0 of the specimen is set to the preheating temperature of 50°C. The heat transfer between the specimen and its surroundings is considered by natural convection (α = 12 W/(m^2·K), Baehr & Stephan, 2011). The heat transfer by radiation ($\varepsilon = \varepsilon_{gapSA} = \varepsilon_{gapSB}$ = 0.7, ibid.) is considered as well.

The FE-mesh consists of 8-node linear brick elements (thermal analysis: DC3D8 in ABAQUS). Close to the welding bead a small element size of approximately 0.5 mm x 0.5 mm perpendicular to the welding direction and 1 mm in welding direction

is chosen (figure 4a). The relevant elements from each welding layer are activated during the simulation as described by Koch and Enderlein (2012). The modelled bead shape is shown in figure 4. The first layer (L1) is approximated as a triangle cross section. Elliptical segments are used for the following layers L2 and L3. The bead shape matches the macrosection as seen in figure 4b.

The heat input during welding is modelled using the Goldak heat source q^{vol} (equation (1)) as described by Koch and Enderlein (2012). The heat source parameters $x_{qf/r}$, y_q, z_q and the arc efficiency η_{arc} which result from calibrating the simulation with temperature measurements are listed in figure 4a. The corresponding heat source domain is marked gray on the example of the second layer.

5. COMPUTATIONAL RESULTS

5.1. Temperature field

The calculation results are validated for the first and second layer of the three pass weld. The computed fusion line and the boundary layer of the HAZ are compared with the corresponding lines out of the macrosection (marked with dotted lines). The temperature range between liquidus and solidus temperature $T_{sol.}$ = 1450°C and $T_{liq.}$ = 1510°C is valid for the fusion line of L485MB acc. to Spur and Stöferle (1987). This range ($T_{sol.} \le T \le T_{liq.}$) is plotted for the intersection plane of the macrosection in figure 5. The computed and observed fusion line of the first layer are in good agreement. The predicted bead shape of the second layer fits the macrosection, but the computed weld bead penetration is slightly smaller than in the macrosection.

The matching for the HAZ is illustrated in figure 6. It is assumed that the temperature range at the boundary layer of the HAZ observed in the macrosection is between $A_{c1start}$ = 720°C and $A_{c3finish}$ = 900°C (acc. to the dilatometric tests). The computed range ($A_{c1start} \le T \le A_{c3finish}$) agrees well with the observed boundary layer for the first and second layer.

The thermocouple measurement loops 2 and 7 are chosen to evaluate the computed thermo cycles, as shown in figure 7. The simulated temperatures are taken from the mesh nodes located at the thermocouple positions. The computational results for thermocouple 7 are in good agreement with the measurement. Here, the difference between calculated and measured temperature is below 4.5%. The

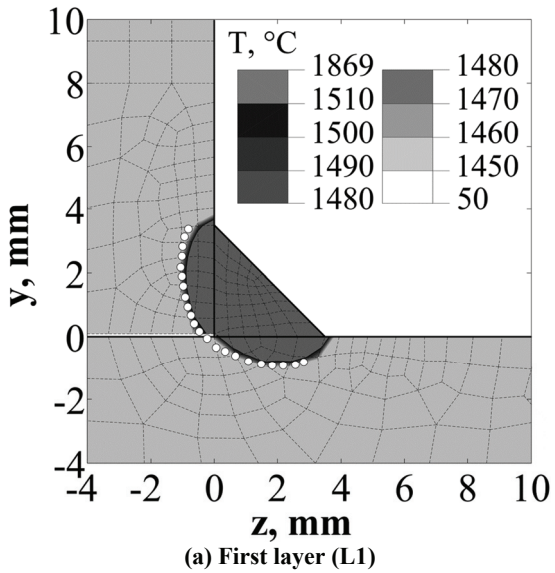

(a) First layer (L1)

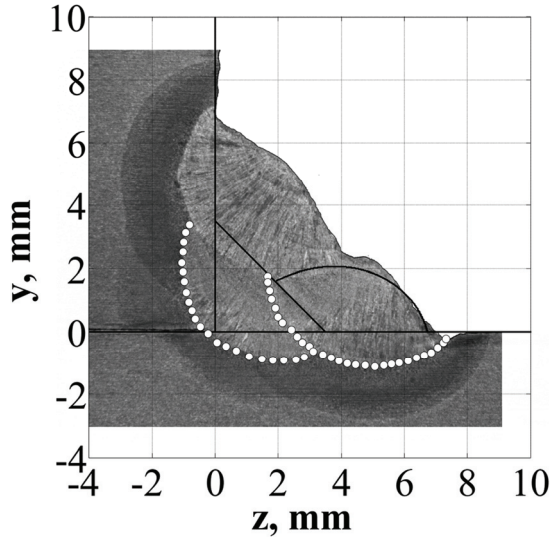

(b) Macrosection at r_2 = 60 mm

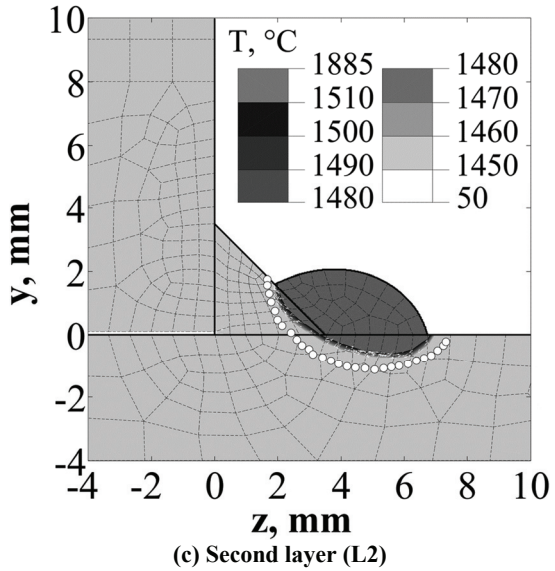

(c) Second layer (L2)

Fig. 5. *Comparison of experimental and calculated results for the fusion line (r_2 cp. figure 2).*

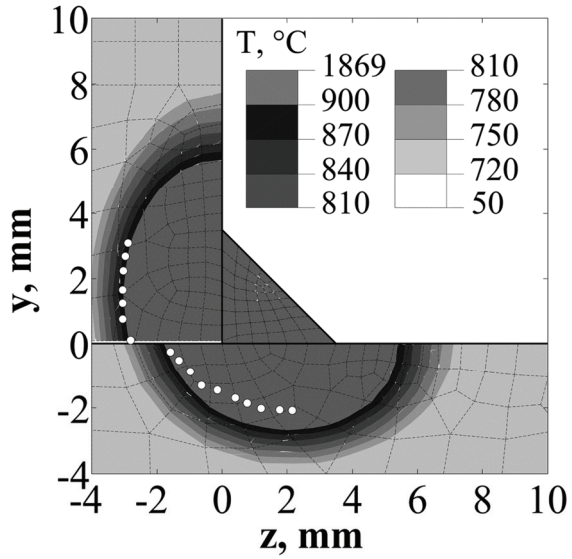

(a) First layer (L1)

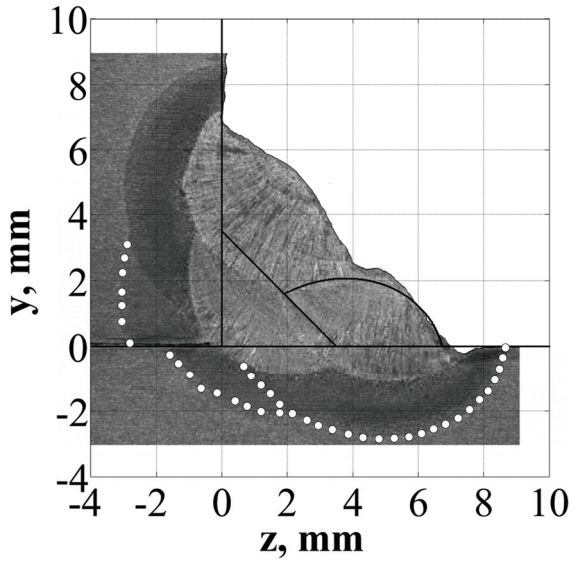

(b) Macrosection at r_2 = 60 mm

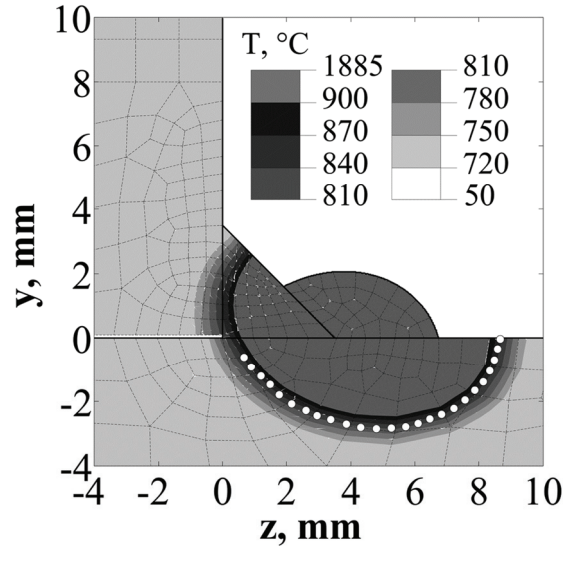

(c) Second layer (L2)

Fig. 6. *Comparison of experimental and calculated results for the HAZ (r_2 cp. figure 2).*

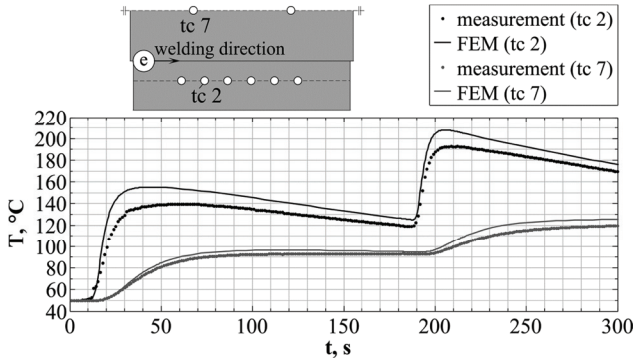

Fig. 7. *Comparison of measured and calculated temperatures.*

predicted temperature curve for thermocouple 2 is slightly higher than the measurement. The calculated local peak temperatures deviate from the measurement by 11% in maximum. However, the cooling velocity at measurement loop 2 is predicted correctly since both the simulated and measured cooling curves run parallel.

5.2. Microstructure

The simulation of microstructure evolution is performed at all nodes in the FE mesh. The initial microstructure is composed of ferrite (80%), pearlite (5%) and bainite (15%). Results for nodes 1, 2 and 3 (figure 8a) are presented in figures 8b, c and d. Nodes 1 and 2 are located in the HAZ of layers 1 and 2, respectively. The reheating effect can be illustrated with node 2. Node 3 is located at the boundary layer of the HAZ. In node 1 86% of martensite is obtained after the 1st cycle and only martensite tempering without changes of phase composition is observed in the 2nd cycle. During heating in the 2nd cycle martensite and bainite in node 2 are transformed into austenite and 85% of martensite is obtained after cooling. In the 1st cycle of node 3 the temperature is below the transformation start temperature. During heating in the 2nd cycle pearlite, bainite and some of the ferrite are transformed into austenite. After cooling 20% of ferrite, 11% of bainite and 69% of martensite are obtained.

6. CONCLUSIONS

The multi-pass welding of L485MB pipeline steel is examined by means of experiment and simulation in order to predict the susceptibility of martensite formation in the HAZ. The temperature field during welding is computed by the FE method. A modified Goldak heat source, calibrated to both layers of the edge fillet weld, is applied to model the heat input. The model

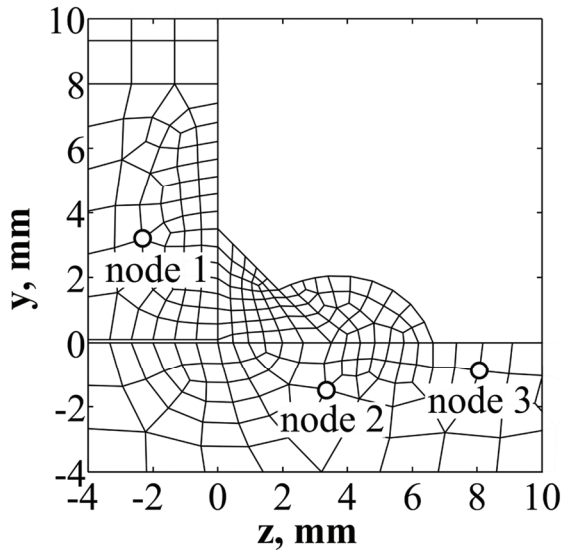

(a)

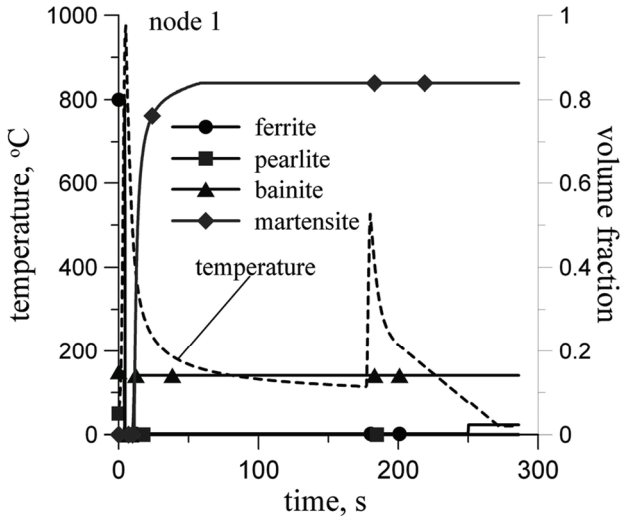

(b)

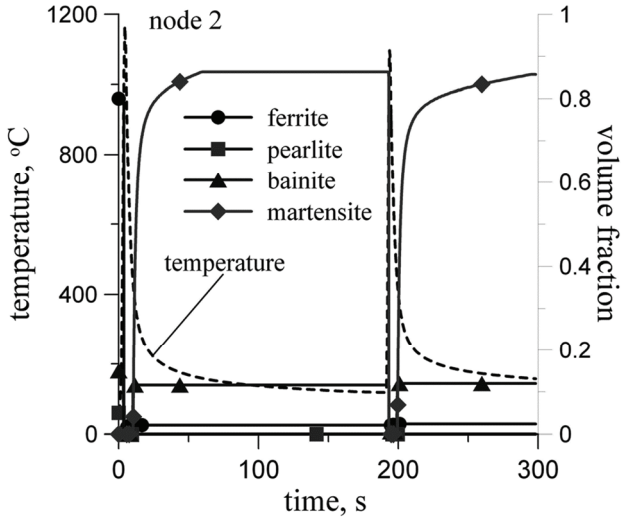

(c)

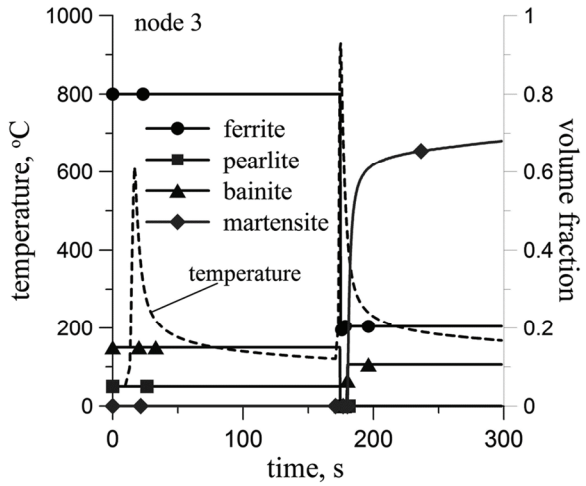

(d)

Fig. 8. *Selected mesh nodes for the microstructure calculation (a) and results (b, c and d)*

provides an acceptable representation of temperatures for both layers. A phase transformation model based on Avrami equation is used to analyze microstructure evolution. The model parameters are adapted to the L485MB pipeline steel. The simulation of the phase transformation show that in the nodes, in which the temperature exceeds 940°C during welding, fully austenitic microstructure is obtained after heating. These nodes are located within the HAZ and the model predicts mainly martensitic microstructure with some bainite and ferrite. Near the boundary layer of the HAZ the maximum temperature is 920°C and 20% of ferrite remains after heating. Here, ferrite (20%), bainite (11%) and martensite (69%) are obtained after cooling.

With respect to the further procedure the influence of the slag on the welding temperature field should be included in the model as explained by Koch and Enderlein (2012). Experiment and simulation has to be extended to analyze the influence of the preheating temperature. Validating the computational results with thermocouple measurements, macrosections as well as microsections is planned.

REFERENCES

Avrami, M., 1939, Kinetics of phase change. I. General Theory, *J. Chem. Phys.*, 7, 1103–12.

Baehr, H. D., Stephan, K., 2011, *Heat and mass transfer*, Springer-Verlag, Berlin.

Donnay, B., Herman, J.C., Leroy, V., Lotter, U., Grossterlinden, R and Pircher, H., 1996, Microstructure evolution of C-Mn steels in the hot deformation process: the stripcam model, *Proc. 2nd Conf. Modelling of Metal Rolling Processes*, eds, Beynon, J.H., Ingham, P., Teichert, H. and Waterson, K., London, 23-35.

Goldak, J.A., Akhlaghi, M., 2005, *Computational welding mechanics*, Springer Science+Business Media Inc, Boston.

Koch, F., Enderlein, M., 2012 Modelling and finite element analysis on multi-pass welding, *Comput. Methods Mater. Sci.*, 12, no. 2, 104-112.

Lan, L., Qiu, C., Zhao, D., Li, C., Gao, X., Du, L., 2011, Microstructural characters and toughness of different subregions in the welding heat affected zone of low carbon bainitic steel, *Acta Metall. Sin.*, 47, 1046-1054.

Li, C., Wang, Y., Han, T., Han, B., Li, L., 2011, Microstructure and toughness of coarse grain heat-affected zone of domestic X70 pipeline steel during in-service welding, *J. Mat. Sci.*, 46, 727-733.

Nishida, Y., Droste, W., Engler, S., 1986, The air-gap formation process at the casting-mold interface and the heat transfer mechanism through the gap, *Met. Trans. B*, 17B, 833-844.

Pietrzyk, M., Madej, L., Koch, F., Enderlein, M., 2010, *Determination of phase transformation models and data for the considered weld materials*, subcontract to the Research project No. 04080238, TU Bergakademie Freiberg, (not published).

Pietrzyk, M., Kuziak, R., 2012, Modelling phase transformations in steel, in: *Microstructure evolution in metal forming processes*, eds, Lin, J., Balint, D., Pietrzyk, M., Woodhead Publishing, 145-179.

Scheil, E., 1935, Anlaufzeit der Austenitumwandlung. *Archiv für Eissenhütt.*, 12, 565-567.

Spur, G., Stöferle, T., 1987, *Handbuch der Fertigungstechnik Band 4/2 Wärmebehandeln*, Carl Hanser Verlag, München (in German).

Szeliga, D., 2012, Selection of the appropriate phase transformation model for design of laminar cooling and continuous annealing of DP steels, *Comput. Methods Mater. Sci.*, 12, 70-84.

Zhang, W., Elmer, J.W., DebRoy, T., 2005, Integrated modelling of thermal cycles, austenite formation, grain growth and decomposition in the heat affected zone of carbon steel, *Sci. Technol. Weld. Join.*, 10, 574-582.

SYMULACJA ROZKŁADU TEMPERATURY I ROZWOJU MIKROSTRUKTURY PODCZAS WIELOWARSTWOWEGO SPAWANIA STALI L485MB DO PRODUKCJI RUROCIĄGÓW

Streszczenie

W niniejszej pracy numeryczna symulacja jest zastosowana jako wstępne narzędzie wspomagania projektowania, optymalizacji i oceny połączeń spawanych w aspekcie ich bezpieczeństwa. Przykładowym zastosowaniem takich połączeń są rurociągi, w których jakość spawu odgrywa istotną rolę. W pracy skupiono się na wielowarstwowych połączeniach spawanych wykonywanych w celu zwiększenia długości lub naprawy rurociągów ze stali L485MB. Stal L485MB (X70) jest powszechnie stosowana na rurociągi o dużej średnicy do transportu gazów i cieczy pod dużym ciśnieniem. Wykonane symulacje przewidywały pola temperatury i rozwój mikrostruktury podczas spawania i chłodzenia po spawaniu. Wielostopniowe ręczne spawanie elektryczne symulowano za pomocą metody elementów skończonych (MES) wykorzystując program ABAQUS. W tym programie jako warunek brzegowy zaimplementowano podwójnie elipsoidalne źródło ciepła opisane modelem Goldaka. Aby uwzględnić różne kształty elektrody model Goldaka został zmodyfikowany poprzez rzutowanie go na kształt elektrody dla każdego przejścia przy spawaniu. Model rozwoju mikrostruktury zaimplementowany w procedurach post-processingu pozwolił na obliczanie kinetyki przemian fazowych w warunkach spawania. Przemiany ferrytyczna, perlityczna były symulowane za pomocą zmodyfikowanego równania Avrami'ego. Wpływ nagrzewania w czasie spawania w wielu przejściach został uwzględniony w obliczeniach. Dla weryfikacji modelu wykonano doświadczalne spawanie. Weryfikacji modelu dokonano przez porównanie zdjęć makro przekrojów i pomiarów temperatury. Zaobserwowano dobrą zgodność pomiarów i obliczeń temperatury w strefie wpływu ciepła.

Received: October 28, 2012
Received in a revised form: November 3, 2012
Accepted: November 6, 2012